RSC Advances

RSC Advances

www.rsc.org/advances

ROYAL SOCIETY OF CHEMISTRY

www.rsc.org/advances

RSC Advances

PAPER

Porous metal–organic framework MIL-100(Fe) as an efficient catalyst for the selective catalytic reduction of NO$_x$ with NH$_3$†

Peng Wang,[a] Huimin Zhao,[a] Hong Sun,[b] Hongtao Yu,[a] Shuo chen,[a] Xie Quan *[a]

The development of an efficient catalyst with excellent catalytic activity and high SO$_2$ resistance at low temperatures (<300 ℃) remains a challenge for the selective catalytic reduction (SCR) reaction. In this study, we report that MIL-100(Fe) is an alternative catalyst for the SCR of NO$_x$ with NH$_3$, and it exhibits higher NO$_x$ conversion than the conventional V$_2$O$_5$-WO$_3$/TiO$_2$ catalyst below 300 ℃. In addition, the effect of H$_2$O and SO$_2$ on the catalytic activity is reversible, and NO$_x$ conversions are recovered after ceasing the flow of SO$_2$ and H$_2$O. *In situ* diffuse reflectance infrared Fourier transform spectroscopy results indicate that both ionic NH$_4^+$ and coordinated NH$_3$ existed on MIL-100(Fe) and that the reaction primarily followed the Langmuir-Hinshelwood mechanism, in which NH$_4^+$ reacts with NO$_2$ formed from NO oxidation over iron sites. Furthermore, the redox properties of the iron species (Fe^{3+}+e$^-$ ↔Fe^{2+}) could play a significant role in activating the reactants.

1. Introduction

The selective catalytic reduction (SCR) of NO$_x$ with NH$_3$ is an efficient method for removing NO$_x$ from stationary sources.[1-3] In practice, the most widely used catalyst for this process is V$_2$O$_5$-WO$_3$(MoO$_3$)/TiO$_2$, which is effective at high operating temperatures (300-400 ℃).[3] Therefore, the SCR unit must be located upstream from the electrostatic precipitator. However, this placement accelerates the deactivation of the catalyst due to the high concentrations of SO$_2$ and ash. In addition, this type of catalyst is still not satisfactory due to the volatility and toxicity of vanadium as well as the high rate of conversion of SO$_2$ to SO$_3$.[4] Therefore, substantial research has been devoted to the development of new vanadium-free catalysts for low temperature SCR (<300 ℃) such that the SCR unit can be located downstream of the electrostatic precipitator and desulfurizer.

At present, the development of efficient SCR catalysts especially low temperature catalysts causes extensive attention. The transition metal oxide supported catalysts or combined catalysts as Ce-based catalyst, Cu-based catalysts, and Mn-based catalysts displayed good catalytic activity compared with

a School of Environmental Science and Technology, Dalian University of Technology, Key Laboratory of Industrial Ecology and Environmental Engineering (Ministry of Education, China) Dalian, 116024, China. E-mail: quanxie@dlut.edu.cn; Fax: +86-411-84706263
b School of Environmental & Chemical Engineering, Dalian Jiaotong University, Dalian 116028, China.
† Electronic Supplementary Information (ESI) available. See DOI: 10.1039/b000000x/

the conventional V$_2$O$_5$-WO$_3$/TiO$_2$ catalysts in the SCR process.[5-10] However, the catalysts exhibit poor SO$_2$ tolerance, especially at relatively low temperature.[11] Therefore, a catalyst with both high activity and high sulfur resistance must be developed.

Metal-organic frameworks (MOFs), which are known to be porous crystalline materials with a large surface area, have recently attracted increasing attention as heterogeneous catalysts due to their unique properties (i.e., high metal content and porosity).[12] MOFs have an infinite network structure constructed of multitopic organic ligands and metal ions, and the pore structure can be customized using the appropriate linkers.[13] The high degree of tunability along with a high surface area and pore topology indicate that MOFs with transition metal centers might serve as potential catalysts for the SCR reaction, especially in the presence of SO$_2$, because the large surface area and porosity are beneficial for dispersing the catalytic components and reducing the accumulation of sulfates on the surface to improve catalytic activity and SO$_2$ resistance.[14] Another important feature that allows MOFs to serve as SCR catalysts is the materials' high metal content; moreover, in MOFs, all of the active sites are ultra-highly dispersed and homogeneous due to the highly crystalline nature of the materials.[15-17] Active sites are freely accessible to reagent molecules. In addition, because the metal ions in MOFs are bonded to organic linkers, the combination of metal cations and organic linkers prevents SO$_2$ poisoning of the active sites.[18]

Therefore, MOFs with transition metals are anticipated to be efficient and sulfur-resistant catalysts for the SCR.

Iron-based catalysts, such as Fe oxides or Fe^{3+} exchange zeolites, are active and environmentally friendly for the NH_3-SCR due to their good activity and N_2 selectivity.[19-21] Therefore, MOFs constructed with iron centers could be an alternative SCR catalyst that exhibits high catalytic activity and high SO_2 resistance. MIL-100(Fe) (MIL: Materials of Institute Lavoisier) is a three-dimensional iron(III) trimesate that is composed of trimers of iron octahedra sharing a common vertex μ_3-O; these trimers are linked by benzene-1,3,5-tricarboxylate moieties to form hybrid supertetrahedra.[22] MIL-100(Fe) contains a significant amount of Fe^{III} CUS (coordinatively unsaturated metal sites) and Fe^{II} CUS, which are due to thermal activation in an inert gas flow, that act as Lewis acid sites.[23] These sites facilitate the adsorption of reactants and promote catalysis. In addition, MIL-100(Fe) could kept the stable structure in the condition with the existence of NO_x, NH_3, SO_2, H_2O and CO_2.[24-27] Therefore, MIL-100(Fe) could be a stable catalyst in the SCR reaction condition.[24-26]

In this study, we investigated the feasibility and performance of MOFs as a novel class of catalytic materials for the SCR of NO_x with NH_3 using the MIL-100(Fe) catalyst. Water and sulfur-resistance experiments were also performed to evaluate the durability of the catalyst in the presence of H_2O and SO_2. *In situ* diffuse reflectance infrared Fourier transform spectroscopy (DRIFTS) was employed to explore the mechanism of NO_x removal. To the best of our knowledge, there are no published reports describing the application of MOF materials for the SCR. This work may provide new insight into the design of efficient SCR catalysts with improved activity.

2. Experimental

2.1 Catalyst preparation

MIL-100(Fe) was prepared from the hydrothermal reaction of trimesic acid with metallic iron, HF, nitric acid and H_2O.[22] The molar composition of the reaction mixture was Fe^0 : 1,3,5-BTC: HF: HNO_3 : H_2O=1.0 : 0.67 : 2.0 : 0.6 : 277 (1,3,5-BTC=1,3,5-benzenetricarboxylic or trimesic acid). The reactant mixture was loaded in a Teflon autoclave and maintained at 150 ℃ for 12 h. The as-synthesized MIL-100(Fe) was further purified by a two-step treatment using hot deionized water (80 ℃) and ethanol (60 ℃) for 3 h. Finally, the resulting light-orange solid was dried at 100 ℃ overnight.

The conventional catalyst (i.e., V_2O_5-WO_3/TiO_2 (V: ~1%, W: ~9%)) was prepared using the incipient wetness method.[2] In a typical preparation, WO_3 was added to a TiO_2 support by impregnation with an aqueous solution of ammonium paratungstate complexed with citric acid, followed by drying and calcination at 550 ℃ for 3 h. Then, vanadium was added to the WO_3/TiO_2 system by impregnation starting from a water solution of ammonium metavanadate and oxalic acid, followed by drying and calcination at 550 ℃ for 2 h.

2.2 Characterization

Powder X-ray diffraction (XRD) patterns were recorded over the range of 3-40 ° on a Panalytical/Empyrean X-ray diffractometer with Cu Kα radiation. Infrared reflectance (IR) spectrums were recorded on a Bruker VERTEX 70 FTIR spectrometer equipped with DTGS detector in the range of 4000-600 cm^{-1} with the resolution of 4 cm^{-1}. The morphology of MIL-100(Fe) was observed using a field-emission scanning electron microscope (SEM, Hitachi S-4800) operated at an accelerating voltage of 10 kV. The specific surface area was determined from a nitrogen adsorption isotherm using the Brunauer-Emmett-Teller (BET) model in Quantachrome SI. Thermogravimetric (TG) analysis was performed using a TG/DTA 6300 thermogravimetric analyzer from Seiko under an air stream (100 ml/min) at a heating rate of 5 ℃/min from 25 to 600 ℃. X-ray photoelectron spectroscopy (XPS) was conducted on the surface analysis system (Thermal ESCALAB 250) using Al Kα radiation. The C 1s peak at 286.4 eV was used for the binding energy calibration.

In situ DRIFTS measurements were performed on a Bruker VERTEX 70 FTIR spectrometer equipped with a MCT detector cooled by liquid nitrogen. An approximately 10 mg sample was finely ground and pressed into a self-supported wafer. The total gas flow was maintained at 100 ml/min by mass flow controllers. Prior to each experiment, the sample was pretreated at 250 ℃ for 10 h and cooled to room temperature in a flow of N_2. At each temperature, the background spectrum was recorded in flowing N_2 and automatically subtracted from the sample spectrum obtained at the same temperature. In the experiment, DRIFT spectra were recorded by accumulating 16 scans at a resolution of 4 cm^{-1}.

2.3 Measurement of catalytic activity

SCR reaction tests were performed in a fixed-bed quartz tube reactor (Φ=9 mm) containing approximately 0.25 g of MIL-100(Fe) and 0.46 g of V_2O_5-WO_3/TiO_2. The MIL-100(Fe) catalyst was pretreated in N_2 at 250 ℃ for 10 h prior to the activity measurement. The feed gas consisted of 500 ppm NO, 500 ppm NH_3, 4% O_2, 500 ppm SO_2 (when used), 5% H_2O (when used), and N_2 balance. The total flow rate was 315 ml/min, and the gas hourly space velocity (GHSV) was 30,000 h^{-1}. The inlet and outlet NO_x (NO plus NO_2) concentrations were analyzed using a flow gas analyzer (ecom-J2KN, rbr Messtechnik GmbH Inc.). The concentration of NH_3 was recorded through by NH_3 analyzer (GXH-1050, Beijing), and the N_2O concentration was monitored by a gas chromatograph (Shimadzu GC-14C) with a Porapak Q column. NO_x conversion and N_2 selectivity were calculated as follows:

$$NO_x \text{ conversion } = \frac{(NO_x)_{inlet} - (NO_x)_{outlet}}{(NO_x)_{inlet}} \times 100\% \quad \text{(Eq. 1)}$$

$$N_2 \text{ selectivity} = \frac{(NO_x + NH_3)_{inlet} - (NO_x + NH_3)_{outlet} - 2N_2O}{(NO_x + NH_3)_{inlet} - (NO_x + NH_3)_{outlet}} \times 100\%$$

(Eq. 2)

The conversion rate was calculated from the conversion of NO_x by using the pseudo-first-order kinetic equation as below.[27]

$$r = -F/W \times \ln(1-x) \quad (\text{mol } NO_x \text{ g cat}^{-1} \text{ s}^{-1}) \qquad \text{(Eq. 3)}$$

In the equation, F is the flow rate of NO (mol s^{-1}), W is the weight of the catalyst (g) and x is NO_x conversion (%).The conversion rate is affected by the reactant concentration, and in this equation the reaction orders of the reactant concentration with respect to NO, NH_3 and H_2O were first order, zero order and zero order, respectively. And the effect of O_2 on the reaction rate is neglected due to its excessive concentration in the reaction.

3. Results and discussion

3.1 Physical and textural properties of MIL-100(Fe) catalyst

MIL-100(Fe) crystallizes in the cubic space group Fd-3m (NO. 227) with the cell parameter of a = 73.340 Å and V= 394481.1 Å^3.[22] Rietveld refinement plot for the XRD pattern of the as-synthesized MIL-100(Fe) was obtained by using the GSAS software.[28] The results demonstrated that the peak positions matched well with that of the simulated diffraction pattern of MIL-100(Fe) in the range of 3 to 40 degree, which indicated that the crystalline state of the sample was consistent with MIL-100(Fe). (ESI†, Figure S1) The SEM image indicated the size of the octahedral crystal, which was approximately 1.5 μm, as shown in Figure 1a. The specific surface area and pore volumes determined by N_2 physisorption were 2032 m^2/g and 1.12 cc/g, respectively, greater than those of the conventional metal oxide catalyst. Therefore, MIL-100(Fe) could provide a high surface area, which is beneficial for the SCR reaction.[29] In addition, the thermal stability of MIL-100(Fe) was studied by TG analysis from 25 to 600 ℃ in air, and the results are shown in Figure S2. A weight loss of 14.5% below 200 ℃ was due to the removal of physically and chemically adsorbed water.[30] The loss observed at 200-300 ℃ was only 2.7%, which indicated that MIL-100(Fe) was thermally stable blow 300 °C. This thermal stability could ensure the applicability of the MIL-100(Fe) catalyst over this temperature range.
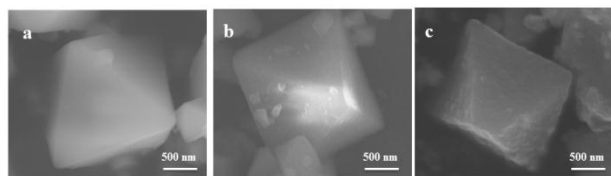
Figure 1. SEM image of MIL-100(Fe). a) MIL-100(Fe) before NH$_3$-SCR activity test; b) MIL-100(Fe) after 20 h NH$_3$-SCR activity test at 250 ^{o}C; c) MIL-100(Fe) after NH$_3$-SCR durability test of resistance of SO$_2$ and H$_2$O at 250 ^{o}C.

3.2 Catalytic performance

3.2.1 NH$_3$-SCR performance. Figure 2a shows the NO_x conversions of the NH$_3$-SCR reaction as a function of temperature over the MIL-100(Fe) and conventional V$_2$O$_5$-

WO$_3$/TiO$_2$ catalysts. The NO_x conversion over MIL-100(Fe) rapidly increased when the temperature was higher than 150 ℃, and a NO_x conversion of more than 97% was obtained at 245-300 ℃. However, the NO_x conversion was only 51%-90% within this temperature range over the V$_2$O$_5$-WO$_3$/TiO$_2$ catalyst. As shown in Figure 2, more than 90% NO_x conversion for the V$_2$O$_5$-WO$_3$/TiO$_2$ catalyst was achieved above 300 ℃. These results indicated that the MIL-100(Fe) catalyst was more active than the conventional V$_2$O$_5$-WO$_3$/TiO$_2$ catalyst for the SCR of NO_x at lower temperatures.

Compared with the conventional catalysts reported in the references,[31,32] the conversion rate of 0.74 ×10^{-6} mol NO$_x$ g cat^{-1} s^{-1} (calculated by Eq. 3) over MIL-100(Fe) at 200 ℃ is greatly higher than those of 0.09 ×10^{-6} mol NO$_x$ g cat^{-1} s^{-1} and 0.13 ×10^{-6} mol NO$_x$ g cat^{-1} s^{-1} over V$_2$O$_5$-WO$_3$/TiO$_2$ catalysts, which indicated MIL-100(Fe) catalyst was more efficient than that of the V$_2$O$_5$-WO$_3$/TiO$_2$ catalyst in the SCR reaction. (Table 1)
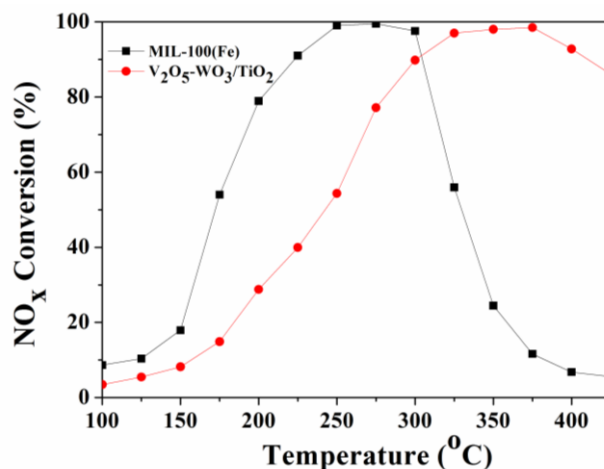
Figure 2. NO$_x$ conversions over MIL-100(Fe) and V$_2$O$_5$-WO$_3$/TiO$_2$. Reaction condition: 500 ppm NO, 500 ppm NH$_3$ and N$_2$ balance, GHSV= 30,000 h^{-1}.

Table 1 Comparison of SCR performance of various catalysts

Catalyst	Temperature (℃)	Rate (mol NO$_x$ g cat^{-1} s^{-1}, 10^{-6})
MIL-100(Fe)	200	0.74
V$_2$O$_5$-WO$_3$/TiO$_2$	200	0.09 (in this work)
V$_2$O$_5$-WO$_3$/TiO$_2$[a,24]	200	0.09
V$_2$O$_5$-WO$_3$/TiO2[b,25]	200	0.13

a. The content of V$_2$O$_5$ is 1 wt%.

b. Commercial catalyst.

However, the catalytic activity of MIL-100(Fe) decreased when the temperature was higher than 300 ℃. The TG analysis results indicated that MIL-100(Fe) began to decompose, and the weight loss increased from 17.2 to 67.5% when the temperature increased from 300 to 405 ℃. SEM images also indicated that MIL-100(Fe) collapsed after the SCR reaction at

325 and 350 ℃ (as shown in Figure S3). The XRD patterns of the samples used are shown in Figure S4. For the sample used at 300 ℃, the typical MIL-100(Fe) phase was still the primary phase. In addition, the Fe_2O_3 phase was detected (2θ = 33.2 and 35.6° (PDF#33-0664)) for the two samples used at 325 and 350 ℃. All of these results indicate that the decrease in NO_x conversion may have been due to the gradual decomposition of the MIL-100(Fe) structure above 300 ℃. In addition, the N_2 selectivity was maintained at 100% over the temperature range of 100-260 ℃. However, as the reaction temperature increased from 260 to 300 ℃, the selectivity rapidly decreased, which generated increasing amounts of the unwanted N_2O by-product (Figure S5a). For V_2O_5-WO_3/TiO_2 catalyst, only 95% of the selectivity to N_2 was obtained when the high NO_x conversion occurred at 350 ℃. (Figure S5b) The concentration of N_2O over MIL-100(Fe) could not be detected in the active temperature range of 225-260 ℃ (NO_x conversion > 90%), For V_2O_5-WO_3/TiO_2 catalyst, it increased from 11 ppm to 63 ppm in the temperature range of 300-400 ℃. These results indicated MIL-100(Fe) exhibited the higher selectivity to N_2 than the conventional V_2O_5-WO_3/TiO_2 catalyst at similar conversions in the SCR process.

3.2.2 Effect of SO_2 and H_2O. Because the existence of H_2O and SO_2 are unavoidable in the exhaust, it is important to investigate the effect of H_2O and SO_2 on the SCR activity of the catalyst. As shown in Figure 3, the NO_x conversion is maintained at approximately 98% in the absence of H_2O and
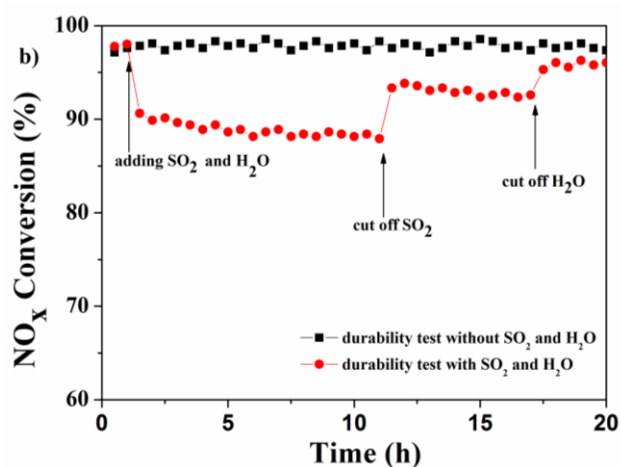
Figure 3. The stability tests of SCR reaction at 250 °C over MIL-100(Fe). Reaction condition: 500 ppm NO, 500 ppm NH_3, 500 ppm SO_2 (when used), 5% H_2O (when used), 4% O_2 and N_2 balance, GHSV= 30,000 h^{-1}.

SO_2. When 500 ppm of SO_2 and 5% H_2O were introduced, the NO_x conversion decreased to 90% and a NO_x conversion of 88% over MIL-100(Fe) catalyst could be obtained after 10 h. It could be attributed to the competitive adsorption between SO_2 and reactants and the formed sulfate depositing on the surface of catalyst and then inhibiting the catalyst activity. After terminating the introduction of SO_2, the conversion of NO_x was restored to 93%, and high NO_x conversion greater than 91% was achieved after 6 h. After cutting off the supply of H_2O, the

NO_x conversion raised to 95%. These results demonstrated MIL-100(Fe) catalyst exhibited a good capacity to resist SO_2 and H_2O, and the inhibition of SO_2 and H_2O on MIL-100(Fe) was a reversible process.

SEM images of the catalysts used in the durability test are shown in Figure 1. The images indicate that the octahedral geometrical shape of the catalyst was retained after the durability test with and without SO_2 and H_2O (Figures 1b and 1c). The XRD patterns of the catalysts used are shown in Figure 4a. As the inset of Figure 4a displayed, it was clearly demonstrated the MIL-100(Fe) catalyst were stable in the SCR reaction even with the presence of SO_2 and H_2O because all characteristic peaks of the used catalysts were still observed and the position was not changed compared with the as-synthesized MIL-100(Fe). Furthermore, the patterns of IR spectrum of MIL-100(Fe) catalysts before and after the durability tests were displaced in Figure 4b. The characteristic peaks[24,33] (υ(C-O) at 1634 and 1378 cm^{-1} and υ(C=C) at 1578 and 1453 cm^{-1}) of the used catalysts were similar with the catalyst MIL-100(Fe) before durability test, which was in accord with the results of XRD patterns of the as-synthesized and used MIL-100(Fe) catalysts. The positive peak (curve d) appeared at 1085 cm^{-1} could be attributed to the deposited sulfate[34] on the surface of MIL-100(Fe) catalyst after durability test with SO_2 and H_2O.

The oxidation states of surface elements on MIL-100(Fe) catalysts before and after durability test were characterized using XPS. As shown in Figure 4c, no S 2p band was observed on MIL-100(Fe) catalyst before durability test. After durability test with SO_2 and H_2O, an evident band at 186.6 eV attributed to S 2p[35] was observed and the S content was calculated to be 1.15% (shown in Table 2), implying the formation of sulfure-containing species on the catalyst surface. Moreover, the Fe content in the used catalyst declined compared with the fresh MIL-100(Fe) catalyst. The reason could be attributed to the coverage of the formed sulfate on the iron sites. Furthermore, the C/O ratio of the used MIL-100(Fe) catalyst was similar with that of the fresh MIL-100(Fe). The result indicated the effect of organic coordination (i.e. the residual trimesic acid) in MIL-100(Fe) on the SCR catalytic activity could be ignored.

Table 2 Ration of Fe, C, O, F and S elements on MIL-100(Fe) before and after durability test (wt%)

catalysts	Fe	C	O	F	S
a	4.59	65.85	29.01	0.55	-
b	3.47	65.98	29.26	0.14	1.15

a, MIL-100(Fe) before durability test; b, MIL-100(Fe) after durability test with SO_2 and H_2O

To elucidate the surface acidity on fresh and used MIL-100(Fe), in-situ DRIFT spectra of NH_3 adsorption were recorded. Prior to the test, the catalysts (0.01g) were exposed in NH_3/N_2 (500ppm) for 1h after treating with N_2 for 30 min to evacuate the impurity at 250 ℃, and followed by purging with N_2 for 30 min at 250 ℃ and the results were displayed in Figure S6. The bands appeared at 1735, 1662 and 1455 cm^{-1}

were attributed to asymmetric and symmetric bending vibrations of NH_4^+ species on Brønsted acid sites.[36,37] The bands displayed at 1603, 1296 and 1151 cm^{-1} were assigned to
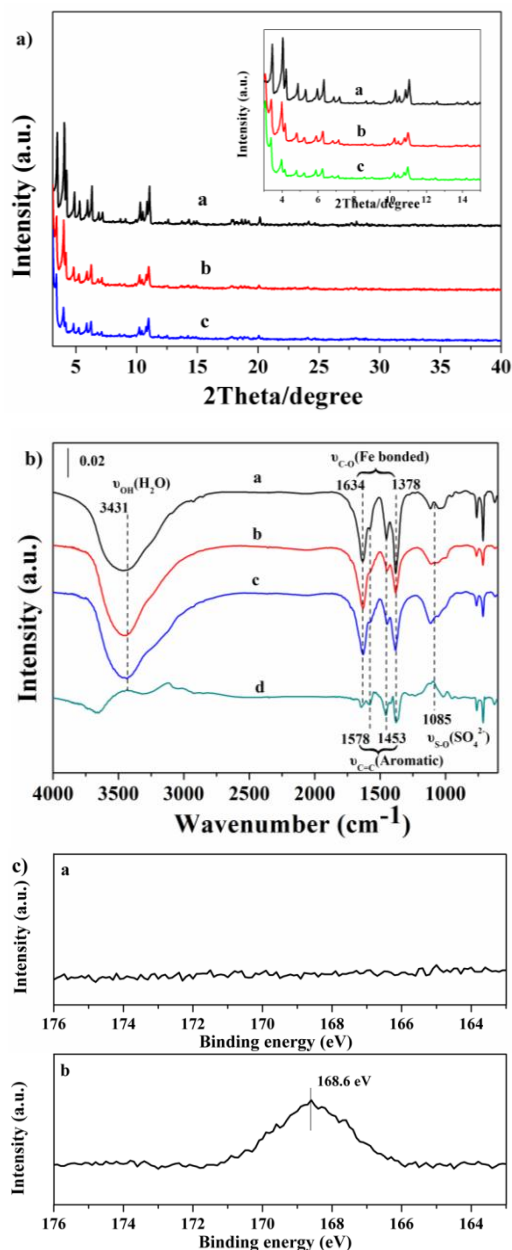
Figure 4. a) Comparison of power X-ray diffraction patterns of various MIL-100(Fe) catalysts: a. before activity test; b. after durability test without SO_2 and H2O; c. after durability test with SO_2 and H_2O; b) Comparisons of IR spectrum of various MIL-100(Fe) catalyst: a. before activity test; b. after durability test without SO_2 and H_2O; c. after durability test with SO_2 and H_2O; d. difference spectra obtained by spectra a subtracting spectra c.; c) XPS spectra of S 2p: a. MIL-100(Fe) before durability test; b. as-synthesized MIL-100(Fe) after durability test with SO_2 and H_2O.

coordinated NH_3 on Lewis acid sites.[38] It is well known the relative quantity of Brønsted acid sites (1735 and 1662 cm^{-1} assigned to $\delta s(NH_4^+)$) and Lewis acid sites (1296 and 1151 cm^{-1} assigned to $\delta s(NH_3)$) on surface of MIL-100(Fe) catalyst could be calculated by the corresponding integral characteristic peak

area. According to Figure S6b, the results indicated both the intensity of B and L acid sites of the used MIL-100(Fe) decreased compared with the fresh MIL-100(Fe). The deposited sulfate on the active sites could prevent the adsorption and activation of gaseous NH_3, which induced the decrease of quantity of acid sites on MIL-100(Fe).

3.3 *In situ* DRIFT studies

To investigate the catalytic reaction mechanism, DRIFTS experiments were performed to identify the species absorbed on the catalyst surface and deduce the surface reaction under actual reaction conditions.

3.3.1 IR spectra of NH_3 adsorption on MIL-100(Fe). Prior to the DRIFT tests, MIL-100(Fe) was first treated at 250 ℃ for 10 h in N_2 and then cooled to 100 ℃ for adsorption of NH_3/N_2. Figure 5 shows the DRIFT spectra of MIL-100(Fe) after it was exposed to 500 ppm NH_3/N_2 from 100 to 275 ℃. The bands at 1735, 1662 and 1455 cm^{-1} were attributed to symmetric and asymmetric bending vibrations of NH_4^+ species on Brønsted acid sites[36,37], and the intensity of these bands increased with temperature above 200 ℃. The bands at 1603, 1296 and 1151 cm^{-1} were assigned to coordinated NH_3 on Lewis acid sites.[38] The observed results were consistent with these as demonstrate in Figure S6. The bands at 3353, 3250 and 3150 cm^{-1} corresponding to N-H stretching were observed.[39] The structure of MIL-100(Fe) is based on μ_3-oxo-centered trimers of octahedral Fe(III). In addition, two of the three octahedral iron atoms are linked by H_2O molecules, and the third iron atom is coordinated to either F$^-$ or OH$^-$ atoms.[22] The anions (OH$^-$) connected to the iron sites can act as Brønsted acid sites. Due to the treatment at 250 ℃ in N_2 for 10 h, some of the coordinated water molecules were removed, and a large number of Fe(III) CUS were formed, which could act as Lewis acid sites.[23,30] In addition, the band at 1506 cm^{-1} was due to the weak adsorption of amide species (NH_2),[40] and the bands at 1551 and 1375 cm^{-1} were assigned to an intermediate formed during the oxidation of ammonia.[41-43]
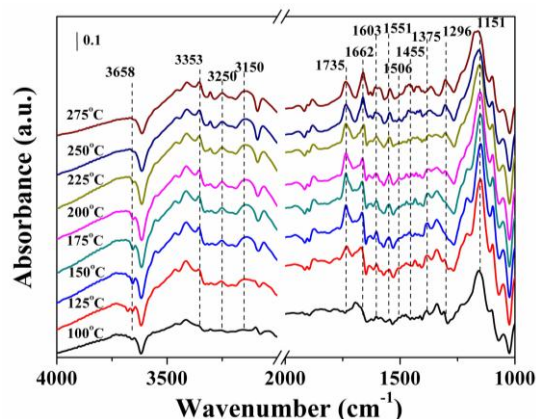
Figure 5. DRIFT spectra of MIL-100(Fe) exposed to NH_3 at various temperatures. Reaction condition: [NH_3] =500 ppm, and N_2 balance.

3.3.2 IR spectra of NO and O_2 adsorption on MIL-100(Fe). NO adsorption on MIL-100(Fe) was investigated by DRIFT

spectroscopy. Figure 6 shows the spectra obtained after the introduction of 500 ppm + 4% O_2 at different temperatures. The bands detected at 1605, 1550, 1278 and 1212 cm^{-1} were attributed to the nitrate species.[44,45] The band at 1901 cm^{-1} was attributed to the nitrosyl group, whose formation could be due to the coordination of a NO molecule to a Lewis acid site of Fe^{3+} via the nitrogen atom.[46] It should be noted that the intensity of the nitrosyl band decreased with increasing temperature and disappeared at 250 ℃. Simultaneously, two new bands at 1624 and 1842 cm^{-1} appeared. The band at 1624 cm^{-1} was due to NO_2 species.[47] According to the results reported in the literature[23], the activation of MIL-100(Fe) at 250 ℃ could form Fe(II) CUS due to the departure of anionic ligands (F$^-$ and OH$^-$). In addition, the band at 1842 cm^{-1} corresponds to the nitrosyl absorbed on Fe^{2+} sites.[46] The results suggested that Fe(III) CUS could be reduced to Fe(II) CUS above 250 ℃ during NO adsorption. In combination with the formation of NO_2, the transformation of the adsorptive species was as follows:

$$Fe^{3+} - NO \xrightarrow{\cdot O} Fe^{2+} - NO_2 \quad\quad\quad (1)$$
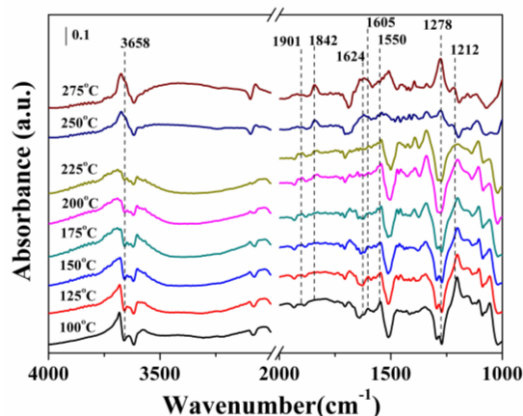
Figure 6. DRIFT spectra of MIL-100(Fe) exposed to NO+O_2 at various temperatures. Reaction condition: [NO] =500 ppm, [O_2] =4 % and N_2 balance.

3.3.3 IR spectra of the reaction species between the adsorbed NH$_3$ species and NO + O$_2$. To understand the SCR reaction mechanism on the surface of MIL-100(Fe), a DRIFT study of the reaction between NO + O_2 and the pre-adsorbed NH_3 species was performed at 250 ℃. In this experiment, the catalyst was first treated with 500 ppm NH_3/N_2 at 250 ℃ for 1 h, followed by N_2 purging for 0.5 h, and then 500 ppm NO + 4% O_2/N_2 was passed over the sample. The DRIFT spectra were recorded as a function of time and are shown in Figure 7. After the introduction of NO+O_2, both bands corresponding to NH_4^+ species and coordinated NH_3 decreased in intensity. This result indicated that both ammonia species, which act as reducing agents, reduce NO_x in the SCR reaction. In addition, the bands assigned to the NH_4^+ species (1735 and 1455 cm^{-1}) disappeared after 4 min, implying that NH_4^+ was prior to react with NO_x compared to the coordinated NH_3. Furthermore, the amide species (NH_2) may be an important intermediate in the SCR reaction because the amide bands immediately disappeared

when NO+O_2 was passed over MIL-100(Fe). The band at 3658 cm^{-1}, which was assigned to H_2O, appeared, and the intensity of this band gradually increased over time. After the active NH_3 species were completely consumed, the nitrate species (1605, 1550 and 1278 cm^{-1}) began to accumulate on the catalyst surface.
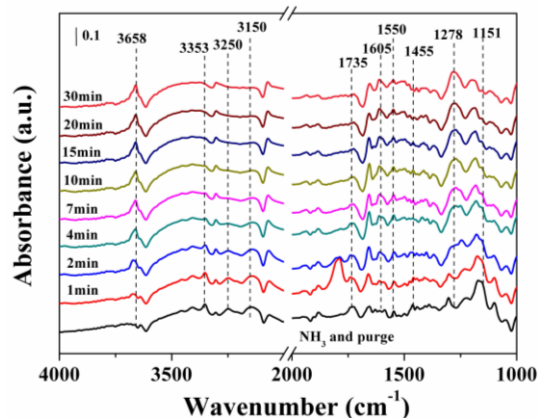
Figure 7. DRIFT spectra of MIL-100(Fe) exposed to NO_x after NH_3 adsorption and purged with N_2 at 250 ^{o}C for various times. Reaction condition: [NH$_3$] =500 ppm, [NO]=500 ppm, [O_2]=4% and N_2 balance .

3.3.4 IR spectra of the reaction species between the adsorbed NO$_x$ species and NH$_3$. A DRIFT study of the reaction between NH_3 and the pre-adsorbed NO_x species on MIL-100(Fe) at 250 ℃ was performed. In this test, the MIL-100(Fe) catalyst was treated with 500 ppm NO + 4% O_2/N_2 at 250 ℃ for 1 h, followed by purging with N_2 for 0.5 h, and then, 500 ppm NH_3 was introduced. The results are shown in Figure 8. The introduction of NH_3 resulted in the rapid disappearance of NO_2 species, which implied that this species was reactive in the SCR reaction. In contrast, the nitrate species (1212 cm^{-1}) were always present on the surface even after 30 min, suggesting that they could have been inactive. Simultaneously, the bands assigned to the coordinated NH_3 (1603, 1296 and 1151 cm^{-1}) and NH_4^+ (1735 and 1662 cm^{-1}) species were observed.
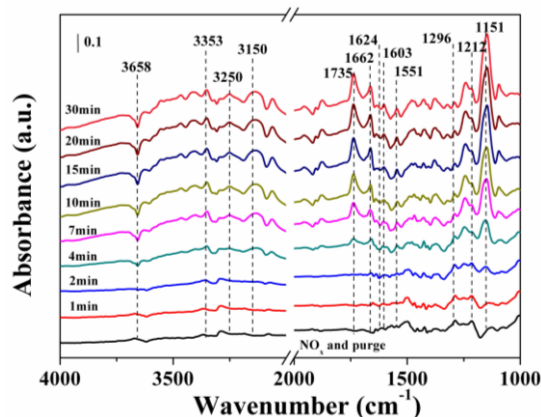
Figure 8. DRIFT spectra of MIL-100(Fe) exposed to NH_3 after NO and O_2 co-adsorption and purged with N_2 at 250 ^{o}C for various times. Reaction condition: [NH$_3$] =500 ppm, [NO]=500 ppm, [O_2]=4% and N_2 balance.

3.3.5 IR spectra of the SCR reaction. To investigate the surface reactive species under realistic SCR reaction conditions, the DRIFT spectra were recorded in a flow of 500 ppm NO+4% O_2 + 500 ppm NH_3 over the MIL-100(Fe) catalyst at 250 ℃. As shown in Figure 9, the bands attributed to the NH_4^+ species (1735, 1662 and 1455 cm^{-1}) and coordinated NH_3 (1603, 1296 and 1188 cm^{-1}) were observed as the reaction time increased. The bands assigned to the NO_x species were not observed during the reaction. The characteristic peaks attributed to H_2O generated from the SCR reaction (3658 cm^{-1}) were detected.
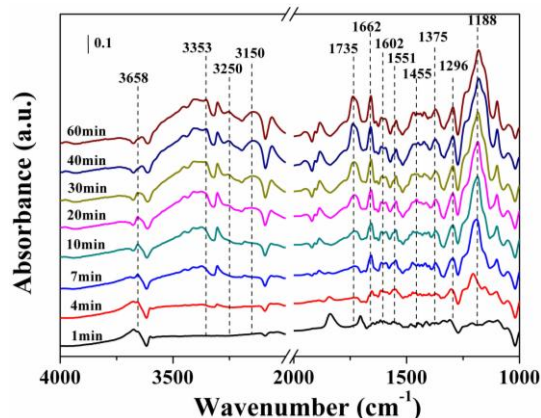
Figure 9. DRIFT spectra of MIL-100(Fe) exposed to the SCR reaction at 250 ^{o}C for various times. Reaction condition: [NH_3] =500 ppm, [NO_x]=500 ppm, [O_2]=4% and N_2 balance.

The DRIFT results for NH_3 adsorption indicated that both Brønsted and Lewis acid sites existed on the surface of MIL-100(Fe), and NH_3 was primarily adsorbed on MIL-100(Fe) in the form of ionic NH_4^+ and coordinated NH_3. In addition, after the introduction of NO+O_2, the disappearance of the NH_4^+ species indicated that ionic NH_4^+ may have been the primary reactive ammonia species adsorbed on MIL-100(Fe) during the reaction.

Because NO was easily oxidized by O_2 on Fe^{3+},[47] NO was adsorbed on the iron sites to form NO_2 species (as described in Section 3.3.2). Then, the reactive NO_2 could react with the neighboring NH_4^+ on the iron sites to form N_2. Therefore, we propose that a Langmuir-Hinshelwood (L-H) mechanism was dominant in the SCR reaction on MIL-100(Fe), as described by the following reaction scheme.

$$NH_3(g) \rightarrow NH_3(a) \rightarrow NH_4^+(a) \rightarrow NH_4^+(a) + NO_2(a) \rightarrow N_2(g) + H_2O(g) \qquad (2)$$
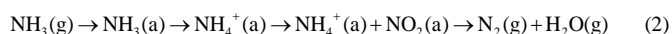
During this process, Fe(III) CUS could be reduced to Fe(II) CUS in the oxidation step of adsorbed NO to NO_2, and then, Fe(II) was reoxidized to Fe(III) by O_2 to complete the redox cycle.

$$Fe^{3+} - NO \xrightarrow{-O} Fe^{2+} - NO_2 + NH_4^+ \longrightarrow N_2 + H_2O + Fe^{2+} \xrightarrow{O_2} Fe^{3+} \qquad (3)$$

The coordinated NH_3 was considered to be less reactive due to the high activation energy required to form NH_2 species.[48] However, based on the results presented in Section 3.3.1, the coordinated NH_3 adsorbed on MIL-100(Fe) could undergo oxidative dehydrogenation to form NH_2 species. In addition, the NH_2 species could react with NO (shown in Figure 5), suggesting that the SCR reaction on MIL-100(Fe) could also occur via the Eley-Rideal (E-R) mechanism.

$$NH_3(g) \rightarrow NH_3(a) \rightarrow NH_2(a) \rightarrow NH_2(a) + NO(g) \rightarrow N_2(g) + H_2O(g) \qquad (4)$$
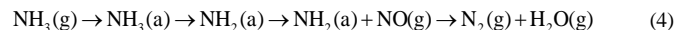
The stable structure of the MIL-100(Fe) catalyst used in the durability test indicated that SO_2 did not easily react with the iron active sites. In addition, the absence of sulfate on the surface of used MIL-100(Fe) catalyst after durability test suggested that the porous structure of MIL-100(Fe) may prevent the deposition of sulfate. Therefore, a high conversion of NO_x could be recovered by eliminating SO_2. The declined NO_x conversion may be attributed to the competitive adsorption between SO_2 and reactants.

4. Conclusions

The porous MOF MIL-100(Fe) catalyst was observed to be an excellent catalyst and exhibited better performance in the SCR of NO_x with NH_3 at lower temperatures (245-300 ℃) than those required by the conventional V_2O_5-WO_3/TiO_2 catalyst. In addition, the MIL-100(Fe) catalyst exhibited satisfactory stability in the presence of H_2O and SO_2 and good self-regeneration capability for the SCR of NO_x after eliminating H_2O and SO_2. XRD, IR and SEM analyses indicated that the structure of the catalyst used in the durability test was the same as that of the fresh sample, suggesting that MIL-100(Fe) was stable during the SCR process below 300 ℃. Based on the DRIFT results, two reaction pathways were proposed. The reaction between the NH_4^+ species and the adsorbed NO_2 species on Fe(II) CUS was the primary reaction pathway, which is consistent with the L-H mechanism. The SCR process also followed the E-R mechanism, through which the amide species reacted with gaseous NO. The valance change of Fe promoted the formation of adsorbed NO_2 species, which were beneficial for the SCR reaction. This study provides insight that may benefit future investigations of MOFs as high-efficiency catalysts in the SCR process. In addition, this work supports the further study of high NO_x conversion over MOFs at low temperature.

Notes and references

1   L.J. Alemany, F. Berti, G. Busca, G. Ramis, D. Robba, G.P. Toledo, M. Trombetta, *Appl. Catal*., *B*, 1996, **10**, 299-311.
2   L. Lietti, I. Nova, P. Forzatti, *Top. Catal.*, 2000, **11/12**, 111-122.
3   L. Lietti, *Appl. Catal.*, *B*, 1996, **10**, 281-297.
4   L. Chen, J. Li, M. Ge, *J. Phys. Chem. C*, 2009, **113**, 21177-21184.
5   W. Shan, F. Liu, H. He, X. Shi, C. Zhang, *Chem. Commun.*, 2011, 4**7**, 8046-8048.

6   J. Xue, X. Wang, G. Qi, J. Wang, M. Shen, W. Li, *J. Catal.*, 2013, **297**, 56-64.

7   P.R. Ettireddy, N. Ettireddy, T. Boningari, R. Pardemann, P.G. Smirniotis, *J. Catal,.* 2012, **292**, 53-63.

8   Y.J. Kim, H.J. Kwon, I. Heo, I. Nam, B.K. Cho, J.W. Choung, M. Cha, G.K. Yeo, *Appl. Catal.*, *B*, 2012, **126**, 9-21.

9   J. Park, H.J. Park, J.H. Baik, I. Nam, C. Shin, J. Lee, B.K. Cho, S.H. Oh, *J. Catal,.* 2006, **240**, 47-57.

10   T. Boningari, R. Koirala, P.G. Smirniotis, *Appl. Catal.*, *B*, 2013, **140-141**, 289-298.

11   W.S. Kijlstra, M. Biervliet, E.K. Poels, A. Bliek, *Appl. Catal.*, *B*, 1998, **16**, 327-337.

12   J.Y. Lee, O.K. Farha, J. Roberts, K.A. Scheidt, S.T. Nguyen, J.T. Hupp, *Chem. Soc. Rev.*, 2009, **38**, 1450-1459.

13   N. Stock, S. Biswas, *Chem. Rev.,* 2012, **112**, 933-969.

14   L.S. Cheng, R.T. Yang, N. Chen, *J. Catal.*, 1996, **164**, 70-81.

15   L.Y. Kong, Z.H. Zhang, H.F. Zhu, H. Kawaguchi, T. Okamura, M. Doi, Q. Chu, W.Y. Sun, N. Ueyama, *Angew. Chem. Int. Ed.*, 2005, **44**, 4352-4355.

16   X.S. Wang, S.Q. Ma, D.F. Sun, S. Parkin, H.C. Zhou, *J. Am. Chem. Soc.*, 2006, **128**, 16474-16475.

17   R.Q. Zou, H. Sakurai, S. Han, R.Q. Zhong, Q. Xu, *J. Am. Chem. Soc.*, 2007, **129**, 8402-8403.

18   S. Han, Y. Huang, T. Watanabe, S. Nair, K.S. Walton, D.S. Sholl, J.C. Meredith, *Microporous Mesoporous Mat.*, 2013, **173**, 86-91.

19   N. Apostolescu, B. Geiger, K. Hizbullah, M.T. Jan, S. Kureti, D. Reichert, F. Schott, W. Weisweiler, *Appl. Catal.*, *B*, 2006, **62**, 104-114.

20   M. Iwasaki, K. Yamazaki, K. Banno, H. Shinjoh, *J. Catal.*, 2008, **260**, 205-216.

21   F. Liu, H. He, C. Zhang, *Chem. Commun.*, 2008, **17**, 2043-2045.

22   P. Horcajada, S. Surblé, C. Serre, D.Y. Hong, Y.K. Seo, J.S. Chang, J.M. Grenèche, I. Margiolaki, G. Férey, *Chem. Commun.*, 2007, **27**, 2820-2822.

23   J.W. Yoon, Y.K. Seo, Y.K. Hwang, J.S. Chang, H. Leclerc, S. Wuttke, P. Bazin, A. Vimont, M. Daturi, E. Bloch, P.L. Llewellyn, C. Serre, P. Horcajada, J.M. Grenèche, A.E. Rodrigues, G. Férey, *Angew. Chem. Int. Ed.*, 2010, **49**, 5949-5952.

24   S. Wuttke, P. Bazin, A. Vimont, C. Serre, Y. Seo, Y.K. Hwang, J. Chang, G. Férey, M. Daturi, *Chem. Eur. J,.* 2012, **18**, 11959-11967.

25   C. Petit, T.J. Bandosz, *Adv. Funct. Mater.*, 2011, **21**, 2108-2117.

26   E. Lenoir, C. Vagner, J.W. Yoon, P. Bazin, F. Ragon, Y.K. Hwang, C. Serre, J. Chang, P.L. Llewellyn, *J. Am. Chem. Soc.*, 2012, **134**, 10174-10181.

27   P. Sazama, B. Wichterlová, E. Tábor, P. Šťastný, N.K. Sathu, Z. Sobalík, J. Dědeček, Š. Sklenák, P. Klein, A. Vondrová, *J. Catal.*, 2014, **312**, 123-138.

28   B. H. Toby, *J. Appl. Cryst.*, 2001, **34**, 210-213.

29   X. Fan, F. Qiu, H.S. Yang, W. Tian, T.F. Hou, X.B. Zhang, *Catal. Commun.*, 2011, **12**, 1298-1301.

30   R. Canioni, C.R. Marchal, F. Sécheresse, P. Horcajada, C. Serre, M. Hardi-Dan, G. Férey, J.M. Grenèche, F. Lefebvre, J.S. Chang, Y.K. Hwang, O. Lebedev, S.Turner, G.V. Tendeloo, *J. Mater. Chem.*, 2011, **21**, 1226-1233.

31   S. Yang, C. Wang, L. Ma, Y. Peng, Z. Qu, N. Yan, J Chen, H Chang, J, Li, *Catal. Sci. Technol.*, 2013, **3**, 161-168.

32   P. Balle, B. Geiger, S. Kureti, *Appl. Catal.*, *B*, 2009, **85**, 109-119.

33   M. Haouas, C. Volkringer, T. Loiseau, G. Férey, F. Taulelle, *J. Phys. Chem. C*, 2011, **115**, 17934-17944.

34   T. Yamaguchi, T. Jin, K. Tanabe, *J. Phys. Chem.*, 1986, **90**, 3148–3152.

35   M.S. Maqbool, A.K. Pullur, H.P. Ha, *Appl. Catal.*, *B*, 2014, **152-153**, 28-37.

36   S.D. Lin, A.C. Gluhoi, B.E. Nieuwenhuys, *Catal. Today*, 2004, **90**, 3-14.

37   B. Jiang, Z. Li, S. Lee. *Chem. Eng. J.*, 2013, **225**, 52-58.

38   G. Ramis, L. Yi, G. Busca, *Catal. Today*, 1996, **28**, 373-380.

39   J.Y. Luo, H. Oh, C. Henry, W. Epling, *Appl. Catal.*, *B*, 2012, **123-124**, 296-305.

40   W.S. Kijlstra, D.S. Brands, E.K. Poels, A. Bliek, *J. Catal.*, 1997, **171**, 219-230.

41   G. Ramis, L. Yi, G. Busca, M. Turco, E. Kotur, R.J. Willey, *J. Catal.*, 1995, **157**, 523-535.

42   M.A. Larrubia, G. Ramis, G. Busca, *Appl. Catal.*, *B*, 2001, **30**, 101-110.

43   M.A. Larrubia, G. Ramis, G. Busca, *Appl. Catal.*, *B*, 2000, **27**, L145-L151.

44   W.S. Kijlstra, D.S. Brands, E.K. Poels, A. Bliek, *J. Catal,.* 1997, **171**, 208-218.

45   M. Machida, M. Uto, D. Kurogi, T. Kijima, *Chem. Mater.*, 2000, **12**, 3158-3164.

46   S. Wuttke, P. Bazin, A. Vimont, C. Serre, Y. Seo, Y.K. Hwang, J. Chang, G. Férey, M. Daturi, *Chem. Eur. J,.* 2012, **18**, 11959-11967.

47   R.Q. Long and R.T. Yang, *J. Catal.*, 2002, **207**, 224-231.

48   G. Qi, R.T. Yang, *J. Phys. Chem. B*, 2004, **108**, 15738-15747.